nature neuroscience

TECHNICAL REPORT

https://doi.org/10.1038/s41593-018-0077-5

Corrected: Author Correction

CRISPR interference-based specific and efficient gene inactivation in the brain

Yi Zheng[1,4], Wei Shen[1,4], Jian Zhang[2], Bo Yang[1], Yao-Nan Liu[1], Huihui Qi[1], Xia Yu[1], Si-Yao Lu[1], Yun Chen[1], Yu-Zhou Xu[1], Yun Li[1], Fred H. Gage[3], Shuangli Mi[2*] and Jun Yao[1*]

CRISPR–Cas9 has been demonstrated to delete genes in postmitotic neurons. Compared to the establishment of proliferative cell lines or animal strains, it is more challenging to acquire a highly homogeneous consequence of gene editing in a stable neural network. Here we show that dCas9-based CRISPR interference (CRISPRi) can efficiently silence genes in neurons. Using a pseudotarget fishing strategy, we demonstrate that CRISPRi shows superior targeting specificity without detectable off-target activity. Furthermore, CRISPRi can achieve multiplex inactivation of genes fundamental for neurotransmitter release with high efficiency. By developing conditional CRISPRi tools targeting synaptotagmin I (*Syt1*), we modified the excitatory to inhibitory balance in the dentate gyrus of the mouse hippocampus and found that the dentate gyrus has distinct regulatory roles in learning and affective processes in mice. We therefore recommend CRISPRi as a useful tool for more rapid investigation of gene function in the mammalian brain.

In recent years, by means of temporally precise optogenetic approaches to acutely manipulate neuronal activity, the functions of neuronal genes and neural circuits in various animal behaviors such as learning and mental processes have been elegantly elucidated. For example, the hippocampus has been demonstrated to play important roles in the control of emotions[1,2]. Whether the emotional changes resulting from acute hippocampal activity adjustment are solely short-term responses to external stimulation or represent a progression toward a stable change in cognitive behavior is less clear. Although conditional recombination systems, such as *Cre–loxP* and FLP–FRT, have been widely used to study the brain with spatiotemporal accuracy, they still present challenges in the form of laborious and time-consuming animal model construction and unexpected animal developmental deficiencies. We suggest that there is a need for neuronal genome-regulating approaches that fall between acute optogenetics and conditional recombination systems to facilitate rapid gene function studies.

Cas9 nuclease has been widely used as a powerful genome editing tool for generating transgenic cell lines and animal strains[3–8]. Navigated by a single guide RNA (sgRNA), Cas9 recognizes specific genomic loci of interest and introduces double strand breaks to delete a functional gene[9–11]. CRISPR–Cas9 has also been demonstrated to inactivate genes in postmitotic neurons[12–14]. However, the misexpressed truncated proteins that result from the random repair of cleavage sites may generate differential phenotypes in nondividing neurons. Compared to the establishment of transgenic cell lines or animal strains, modifying genes in the neural network leads to greater challenges, especially due to the demand for homogeneity in postcleavage gene repair and the abolishment of deflected targeting. Recently, an engineered nuclease null form Cas9 (dCas9) has been developed into a versatile tool for gene regulation and imaging of genomic loci or mRNA[15–17]. The dCas9-based CRISPRi approach, in which dCas9 is fused to the transcription repressor KRAB (dCas9-KRAB)[18,19], has been developed to block transcription around a window of the transcriptional start site (TSS), yielding a promising gene knockdown (KD) technology[18–23]. The avoidance of indels would improve genotypic consistency following gene suppression, which would make CRISPRi particularly suitable for inactivating genes in the brain.

In this study, we designed CRISPRi-based KD tools to inactivate a series of genes essential for neurotransmitter release in neurons. We found that CRISPRi can downregulate the expression of all target genes to nearly complete abolishment. Furthermore, using chromatin-immunoprecipitation and quantitative PCR (ChIP-qPCR) analysis, based on a pseudotarget fishing strategy, we demonstrated that CRISPRi has superior targeting specificity without detectable off-target activity in the neuronal application. We developed CRISPRi-based conditional gene KD tools to inactivate *Syt1* in the dentate gyrus (DG) of the mouse hippocampus in a neuronal subtype-specific manner and achieved efficient bidirectional regulation of the excitatory–inhibitory (E-I) balance in this region. We found that the learning competency of the animals could be bidirectionally regulated; however, the mice always showed anxiety- and depression-like behaviors in response to the forward and reverse E-I adjustment. Therefore, the homeostasis of the E-I balance in the DG is essential for the coordination of cognitive behaviors. Finally, we developed two multiplex CRISPRi systems and demonstrated that multiplex CRISPRi was able to abolish five genes that encode a protein complex essential for neurotransmitter release in the brain. Our study demonstrated that CRISPRi enables rapid and accurate gene function investigation in the brain.

Results

CRISPRi inactivates genes in neurons with high applicability and efficiency. dCas9, in which the Asp10 and His840 residues of Cas9 are replaced with alanine, has been shown to prohibit gene expression in dividing cells when conjugated with KRAB, a transcription suppressor[18–23]. dCas9-KRAB is typically guided to the TSS of a gene to block transcription initiation[18,19], whereas Cas9 is mostly targeted to disrupt constitutive 5′ coding exons so that premature termination of transla-

[1]State Key Laboratory of Membrane Biology, Tsinghua-Peking Joint Center for Life Sciences, IDG/McGovern Institute for Brain Research, School of Life Sciences, Tsinghua University, Beijing, China. [2]Key Laboratory of Genomics and Precision Medicine, Beijing Institute of Genomics, Chinese Academy of Sciences, Beijing, China. [3]The Salk Institute for Biological Studies, Laboratory of Genetics, La Jolla, CA, USA. [4]These authors contributed equally: Yi Zheng and Wei Shen. *e-mail: mishl@big.ac.cn; jyao@mail.tsinghua.edu.cn

tion occurs (Fig. 1a). We engineered CRISPRi for neurons by adapting the Cas9 in the lentiCRISPR v2 vector (Addgene #52961) to dCas9 with KRAB conjugated to its N-terminus[18,19,24], as well as replacing the puromycin with an EGFP cassette. We investigated the performance of CRISPRi in cultured hippocampal neurons using *Syt1* and three SNARE genes, *Vamp2*, *Stx1a* and *Snap25*, as experimental models. All four of these genes are vital for neurotransmission. The SNARE proteins can form the minimal fusion machinery for the secretion of neurotransmitters[25,26], and Syt1 is the primary Ca^{2+} sensor for action potential (AP)-evoked fast synchronous neurotransmitter release[27]. We designed sgRNAs with the highest proposed score, targeting the DNA region from −50 to 300 bp relative to the TSS of the genes for KD[18,28]. To evaluate the efficiency of CRISPRi, we investigated three stem–loop short hairpin RNAs (shRNAs) per gene, acquired from the RNAi Consortium library, for parallel comparison[29]. Analyses of quantitative reverse-transcription PCR (qRT-PCR) and immunoblot revealed that all four genes were repressed at the mRNA and protein levels by the designed sgRNAs, approaching more than 90% KD efficiency (Fig. 1b–d). However, compared to CRISPRi, shRNA-based RNAi exhibited an overall moderately inhibiting performance for all tested genes. We carried out whole-cell patch-clamp recording analysis to evaluate the effects of CRISPRi-mediated *Syt1* and SNARE-gene KD on AP-evoked release. The results indicated that in all fully KD groups, the amplitude of the excitatory postsynaptic currents (EPSCs) was greatly reduced (Fig. 1e,f) and that lentiviral reintroduction of exogenous genes, which was simply driven by a synapsin promoter, could rescue the KD phenotype (Fig. 1e,f). Hence, the release of neurotransmitters was substantially diminished following the suppression of these four genes. We note that the *Stx1a*-targeting sgRNA (*Stx1a* sg1) abolished EPSCs in only half of the tested neurons (data not shown), although the overall protein and mRNA levels were both reduced by > 90% (Fig. 1b–d), which might have been caused by functional redundancy of the homolog *Stx1b* gene. We extended the investigation of CRISPRi to more genes, including *Stx1b*, *Doc2a* and *Doc2b*, the latter two of which have been suggested to be the Ca^{2+} sensors for spontaneous and AP-evoked asynchronous forms of synaptic vesicle secretion[30,31]. The results confirmed that CRISPRi always generated highly specific and homogeneous KD efficiencies (Fig. 1d).

CRISPRi has very high targeting specificity. In the next step, we investigated the targeting specificity of dCas9-KRAB in neurons. Using one tested *Syt1*-targeting sgRNA, *Syt1* sg2, as an example, we monitored the time-lapse gene-suppression activity of dCas9-KRAB in neurons during a 14-d observation course (Fig. 2a,b). A *Syt1* shRNA with the highest inhibiting efficiency was used for parallel comparison to determine the temporal efficiency of CRISPRi. We found that, although Syt1 expression was increased in the control group as the neuron matured, dCas9-KRAB with *Syt1* sg2 started to decrease Syt1 expression beginning at 8 d in vitro in a time-dependent manner. RNAi showed functional kinetics similar to those of CRISPRi, but its inhibiting efficiency always lagged behind that of CRISPRi. Using ChIP-qPCR, we investigated the temporal binding of dCas9-KRAB to the *Syt1* locus. The results indicated that the link between dCas9-KRAB and the *Syt1* target site persistently increased throughout the observation window (Fig. 2c). The tight association of dCas9-KRAB with the chromatin was attributed to dCas9 but not KRAB, as the binding of dCas9 to the same locus exhibited a similar affinity.

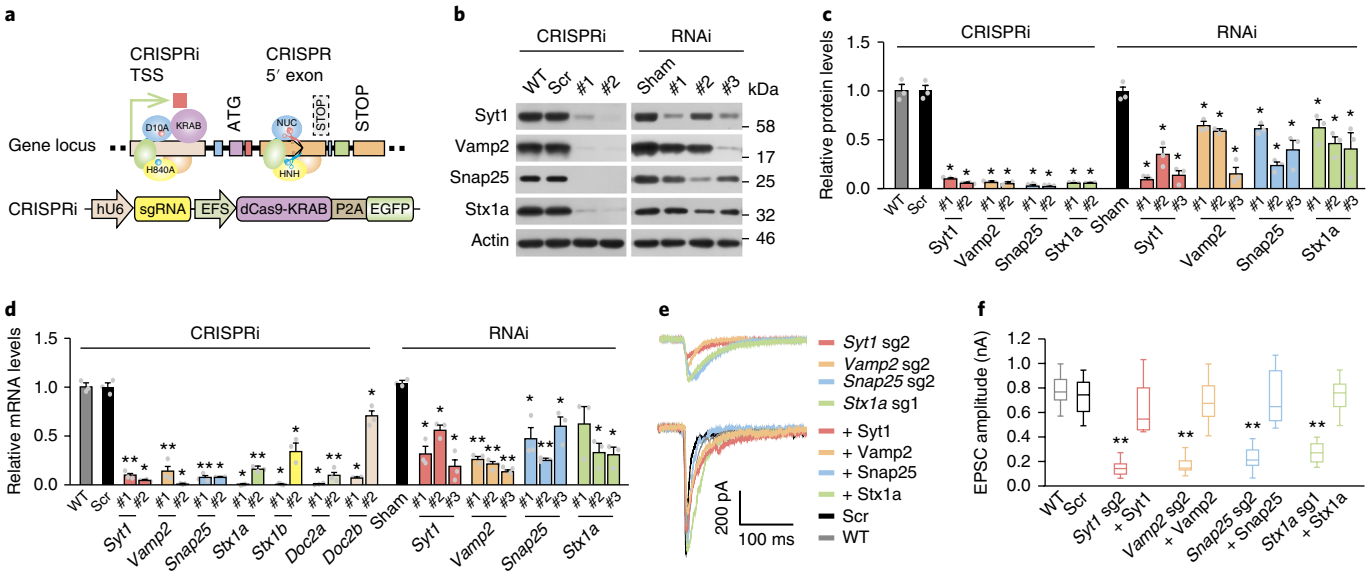

Fig. 1 | CRISPRi efficiently inactivates gene expression in primary neurons. a, Schematic representation of distinct gene inactivation patterns mediated by CRISPRi and CRISPR. In the CRISPRi system, EGFP is cleaved from dCas9-KRAB through the P2A self-cleaving peptide and thus is quantitatively indicative of dCas9-KRAB expression. NUC and HNH are nuclease domains of Cas9; ATG, translational start codon; STOP, translational stop codon; EFS, elongation factor-1α short promoter; EGFP, enhanced green fluorescent protein. **b**,**c**, Immunoblot analysis (**b**) and quantification (**c**) of protein expression in neurons expressing CRISPRi or shRNA-based RNAi ($n = 3$ for all groups). Scr, scrambled sgRNA; #1, #2 and #3 are the indicated sgRNAs of the corresponding gene. In **b**, blots were cropped; full-length blots are presented in Supplementary Fig. 7. **d**, qRT-PCR analysis of mRNA expression in dCas9-KRAB + sgRNA or shRNA infected neurons ($n = 3$ for all groups). In **b**, **c** and **d**, data were obtained from neurons from three independent cultures with similar results and shown as mean ± s.e.m. Statistical significance was assessed by unpaired Student's *t* test. $^*P < 0.05$; $^{**}P < 0.001$. **e**,**f**, Representative traces (**e**) and peak amplitudes (**f**) of AP-evoked EPSCs recorded from WT, CRISPRi-mediated KD and rescued neurons ($n = 25$, 20, 30, 10, 30, 18, 29, 20, 28 and 16). Data were obtained from neurons from three independent cultures with similar results; *n* values represent the numbers of cells analyzed. Quantifications are presented as box-and-whisker plots with upper and lower whiskers representing the maximum and minimum values, respectively; the boxes represent 2.5%, median and 97.5% quartiles. Statistical significance was assessed by unpaired Student's *t* test; $^{**}P < 0.001$. For detailed numbers and statistical analysis, see Supplementary Table 3.

Comparing the protein expression and chromatin binding outcomes of dCas9-KRAB at 8 and 10 d in vitro (Fig. 2b,c), we concluded that CRISPRi needed to reach a high DNA-binding rate threshold (approximately 50%) to generate obvious inhibitory effects. However, if dCas9-KRAB had decent tolerance to DNA mismatch, it might generate severe off-target gene suppression due to its robust DNA binding affinity. To address this concern, we sought to investigate the functioning of dCas9-KRAB at false gene loci with slight differences from the bona fide target. We thus employed a pseudotarget fishing strategy by simulating the wild-type *Syt1* gene as a 'pseudofalse' target (bait) and expressing an array of mismatched sgRNAs (fish) to test whether dCas9-KRAB could efficiently detect and suppress the pseudotarget (Fig. 2d). The *Syt1* sg2 variants were designed by modifying every other nucleotide, starting from the PAM-proximal terminal. ChIP-qPCR analysis revealed that all the *Syt1* sgRNA variants failed to efficiently instruct dCas9-KRAB binding to the *Syt1* locus (Fig. 2e). Consistently, the results of both qRT-PCR and immunoblot analyses indicated that Syt1 expression was unaffected by any of the *Syt1* sg2 variants guiding dCas9-KRAB (Fig. 2f,g). We further investigated three other sgRNAs, including *Syt1* sg1 and *SNAP25* sg1 and sg2, and found that none of the tested sgRNA variants could efficiently bind the target loci or generate effective gene interference (Fig. 2h,i and Supplementary Fig. 1). Hence, dCas9-KRAB was highly resistant to sgRNA or DNA mismatching, thus guaranteeing a high targeting specificity.

Conditional inactivation of Syt1 disturbs the E-I balance in the DG. Rapid disruption of genes in well-defined neuronal subpopulations in specific brain regions should facilitate the understanding of neural circuit functions. As Syt1 is essential for AP-evoked neurotransmitter release, Syt1 selective deficiency in either excitatory or inhibitory neurons should be able to efficiently shift the E-I balance of the neural circuit, thus regulating the output of the DG neural network. Therefore, we devised two conditional CRISPRi tools to silence Syt1 expression in either glutamatergic or GABAergic neurons with dCas9-KRAB expression under the control of pCaMKIIα and pVGAT promoters[32,33], respectively (Fig. 3a). We stereotactically infused lentivirus encoding the *Syt1*-targeted conditional CRISPRi system into the DG (Fig. 3b). Analysis of brain slice immunostaining showed that the majority of pCaMKIIα::dCas9-KRAB$^+$ neurons were confined to the granule cell layer of the DG, spanning from anterior to the posterior DG and accounting for approximately 20% of all DAPI$^+$ cells in the DG (Fig. 3b and Supplementary Fig. 2). To determine the specificity of CRISPRi expression, dCas9-KRAB$^+$ neurons were purified using a fluorescence-activated cell-sorting assay and were then subjected to qRT-PCR analysis (Fig. 3c). We observed highly specific enrichment of the genes encoding vesicular glutamate transporter 1 (*Vglut1*) in pCaMKIIα::dCas9-KRAB$^+$ neurons and glutamic acid decarboxylase 1 (*Gad1*) in pVGAT::dCas9-KRAB$^+$ neurons (Fig. 3d). These results indicated a subtype-specific expression of CRISPRi system in the DG, which is consistent with the immunostaining results of primary cultures (Supplementary Fig. 3). Moreover, Syt1 expression was selectively abolished by conditional CRISPRi within *Syt1*-targeting glutamatergic or GABAergic neurons but not in both, compared to the scrambled sgRNA (Fig. 3e,f). These results indicated that CRISPRi can be adapted for versatile and efficient gene disruption in specific classes of neurons in living animal brains.

We carried out whole-cell patch-clamp recording analysis to evaluate the effects of selective *Syt1* inactivation on the release of neurotransmitters in primary neurons. The results indicated that, in the pCaMKIIα-driving group, Syt1-triggered EPSCs were largely

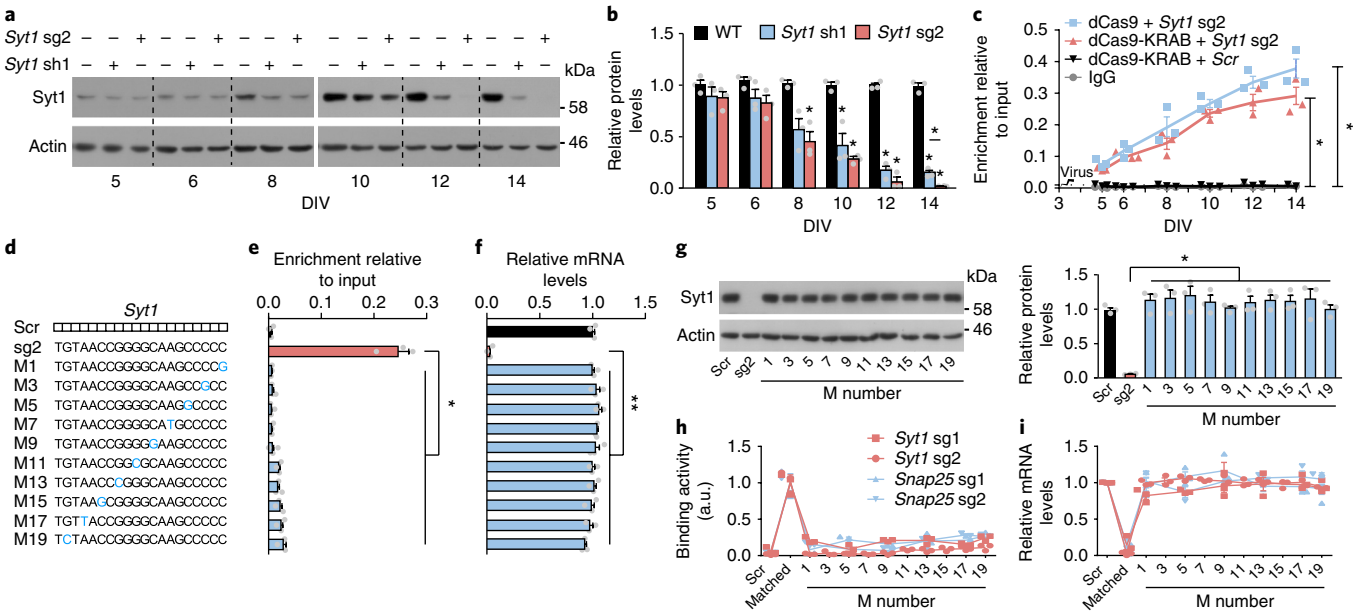

Fig. 2 | CRISPRi shows prominent targeting specificity in neurons. a,**b**, Immunoblot analysis (**a**) and normalized quantification (**b**) of time-lapse expression of Syt1 by CRISPRi- and RNAi-mediated KD ($n = 3$ for all groups). **c**, ChIP-qPCR analysis of dCas9 or dCas9-KRAB binding to the *Syt1* locus during a 14-d window ($n = 3$ for all groups). **d**, Design of *Syt1* sg2 variants to test the binding of dCas9-KRAB to the 'false' *Syt1* gene. M numbers represent the corresponding mismatch in the sgRNA, which is highlighted in blue. **e**, ChIP-qPCR analysis of dCas9-KRAB binding to the *Syt1* locus with the navigation of *Syt1* sg2 variants ($n = 3$ for all groups). **f**, qRT-PCR analysis of *Syt1* mRNA expression in neurons expressing different *Syt1* sg2 variants ($n = 3$ for all groups). **g**, Immunoblot analysis and quantification of Syt1 expression in neurons with co-expression of *Syt1* sg2 variants and dCas9-KRAB ($n = 3$ for all groups). In **a** and **g**, blots are cropped; full-length blots are presented in Supplementary Fig. 7. In **a**–**c** and **e**–**g**, data were obtained from neurons from three independent cultures with similar results and shown as mean ± s.e.m. Statistical significance was assessed by unpaired Student's *t* test; $^*P < 0.05$; $^{**}P < 0.001$. For detailed numbers and statistical analysis, see Supplementary Table 3. **h**,**i**, Summary of ChIP-qPCR analysis of sgRNA array-guided binding of dCas9-KRAB to the *Syt1* and *Snap25* loci (**h**) and the correspondent gene inactivation (**i**). For detailed experiments, see Supplementary Fig. 1; $n = 3$ for all independent experiments.

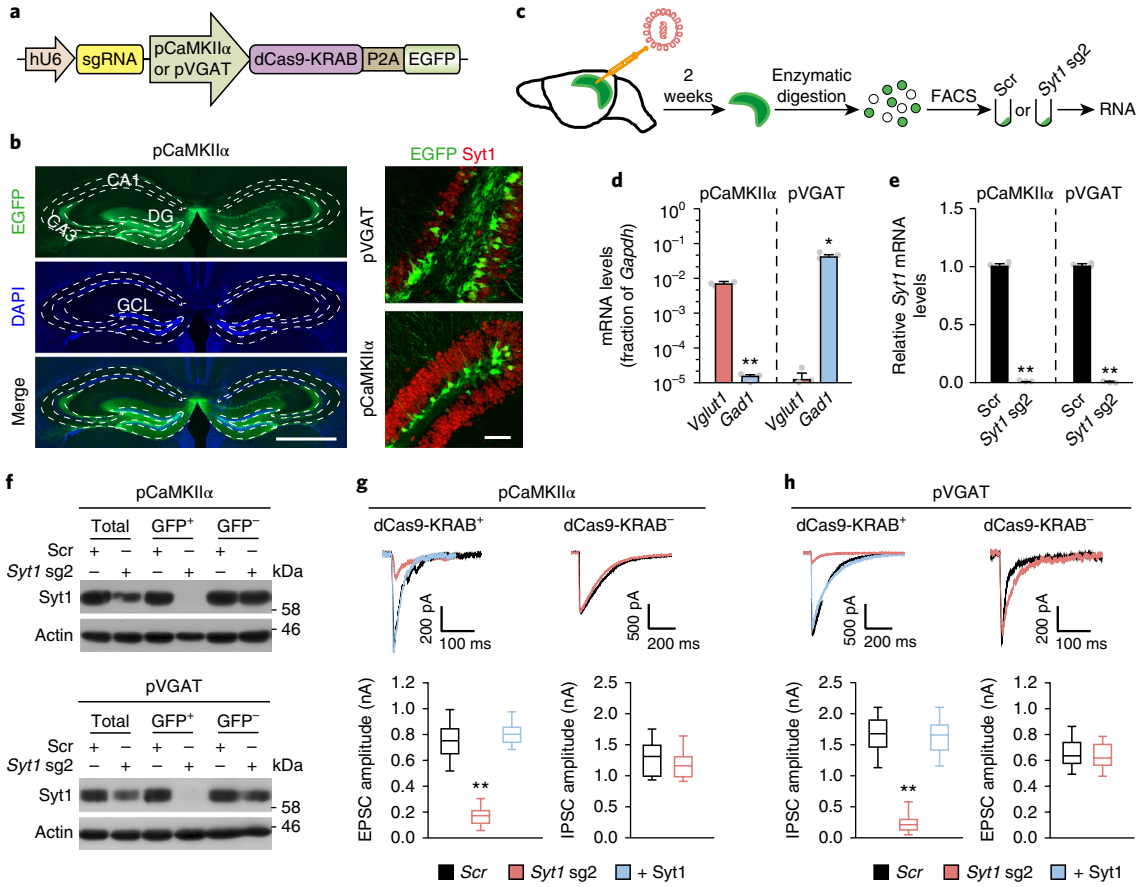

Fig. 3 | CRISPRi-based conditional inactivation of *Syt1* shifts the E-I balance of the DG. a, Schematic demonstration of the conditional CRISPRi system. The mouse pCaMKIIα and pVGAT promoters drive the selective expression of dCas9-KRAB in glutamatergic and GABAergic neurons, respectively. **b**, Representative immunofluorescence images showing expression of CRISPRi in the DG. Left: DG infection with lentiviral CRISPRi; in-vector EGFP indicates dCas9-KRAB expression. Scale bar, 1 mm. Right: pVGAT-driving selective inactivation of Syt1 in GABAergic neurons (top) and pCaMKIIα-driving Syt1 suppression in glutamatergic neurons (bottom). Scale bar, 100 μm. Data were obtained from three mice with similar results. GCL, granule cell layer. **c**, Flowchart showing purification of dCas9-KRAB$^+$ neurons from the mouse brain. FACS, fluorescence-activated cell sorting. **d**, qRT-PCR analysis of *Vglut1* and *Gad1* expression within sorted pCaMKIIα$^+$ or pVGAT$^+$ neurons ($n = 3$ for all groups). **e**, *Syt1* expression in sorted pCaMKIIα$^+$ or pVGAT$^+$ neurons ($n = 3$ for all groups). In **d** and **e**, data were obtained from three mice with similar results and shown as mean ± s.e.m. Statistical significance was assessed by unpaired Student's *t* test; $^*P < 0.05$; $^{**}P < 0.001$. For detailed numbers and statistical analysis, see Supplementary Table 3. **f**, Immunoblot analysis showing selective Syt1 inactivation in pCaMKIIα- (upper panel) or pVGAT-driving (lower panel) neurons. Data were obtained from three mice with similar results. Blots are cropped; full-length blots are presented in Supplementary Fig. 8. **g**, Representative traces (upper panels) and average peak amplitudes (lower panels) of AP-evoked EPSCs (left) in pCaMKIIα$^+$ glutamatergic neurons and IPSCs (right) in noninfected GABAergic neurons ($n = 24, 30, 12, 11, 10$). **h**, Representative traces (upper panels) and average peak amplitudes (lower panels) of AP-evoked IPSCs (left) in pVGAT$^+$ GABAergic neurons and EPSCs (right) in noninfected glutamatergic neurons ($n = 35, 28, 13, 14, 10$). In **g** and **h**, data were obtained from neurons from three independent cultures with similar results; *n* values represent the numbers of cells analyzed. Quantifications are presented as box-and-whisker plots with upper and lower whiskers representing the maximum and minimum values, respectively; the boxes represent 2.5%, median and 97.5% quartiles. Statistical significance was assessed by unpaired Student's *t* test; $^{**}P < 0.001$. For detailed numbers and statistical analysis, see Supplementary Table 3.

abolished in dCas9-KRAB$^+$ glutamatergic neurons compared to scrambled sgRNA, whereas the inhibitory postsynaptic currents (IPSCs) in dCas9-KRAB$^-$ GABAergic neurons remained unchanged (Fig. 3g). Likewise, in the pVGAT-driving group, dCas9-KRAB$^+$ GABAergic neurons exhibited considerably reduced IPSCs within the context of *Syt1*-targeting sgRNA, whereas glutamatergic neuron-generated EPSCs were unaffected (Fig. 3h). It has been suggested that other Ca^{2+} sensors, such as Syt2 and Syt9, may play redundant roles in triggering fast synchronous release in GABAergic neurons[34,35]. In the purified pVGAT-driving dCas9-KRAB$^+$ GABAergic neurons, we found that the mRNA expression of *Syt2* and *Syt9* was very weak in the absence of Syt1 (Supplementary Fig. 4a). We overexpressed exogenous Syt2 and Syt9 in GABAergic neurons and found that their co-expression could rescue the Syt1 KD phenotype in GABAergic neurons (Supplementary Fig. 4b,c). These results indicated that Syt2 and Syt9 were not adequately expressed in *Syt1*-KD GABAergic hippocampal neurons to trigger robust IPSCs. Taken together, our data indicated that conditional inactivation of *Syt1* was able to regulate the excitatory and inhibitory outputs of the neural network.

Tuning of the E-I balance within the DG reveals distinct regulation of cognitive and memory processes. We then evaluated the performance of conditional *Syt1* KD in DG functioning by assaying the memory and cognitive behaviors of the animals receiving CRISPRi-mediated E-I shifting. An open field test revealed that Syt1 depletion in glutamatergic or GABAergic DG neurons did not alter the average speed or locomotion of the animals (Supplementary

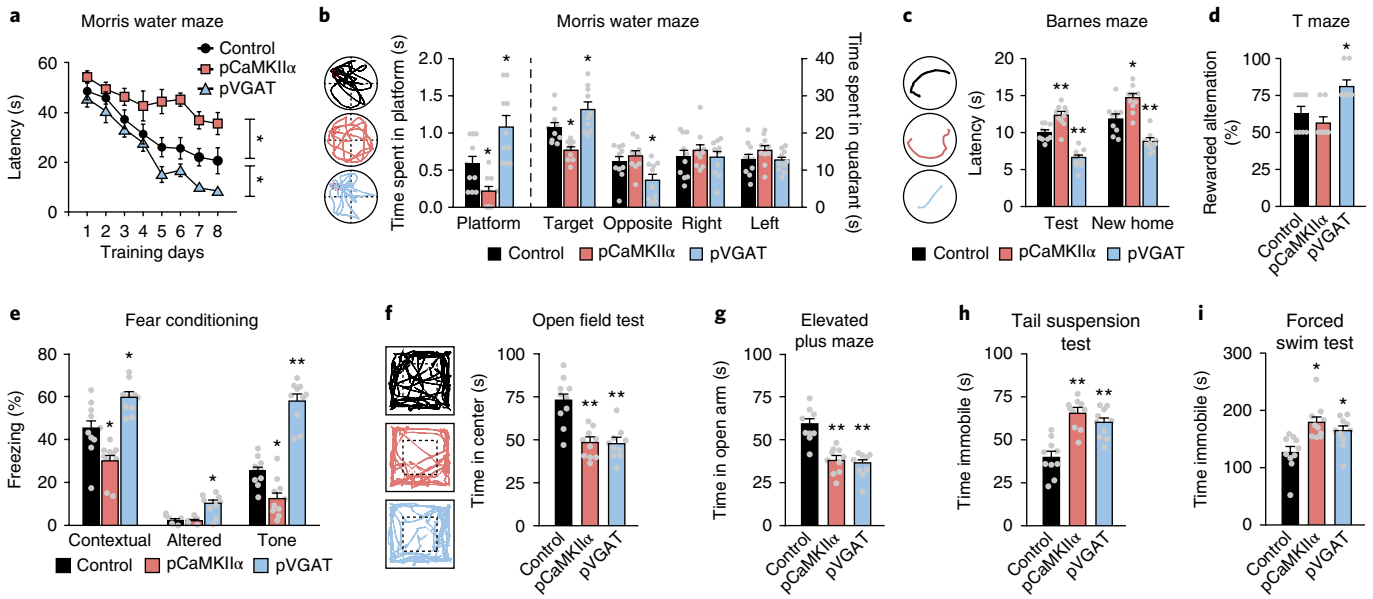

Fig. 4 | Tuning of the E-I balance has distinct learning and mental regulation in the DG. a, Average time spent to locate submerged escape platform during the 8-d training session in the Morris water maze ($n = 10, 10, 10$ mice). **b**, Representative paths (left) and average time (right) spent on the platform and in the four quadrant areas when the platform was absent ($n = 10, 10, 10$ mice). **c**, Representative paths (left) and average latency time (right) spent to locate the original refuge (test) and new refuge (new home) in the Barnes maze test ($n = 10, 10, 10$ mice). **d**, Percentage of correct alternation in the rewarded T maze test ($n = 8, 8, 8$ mice). **e**, Percentage of freezing levels in the training context, altered context and cued tone fear conditioning test ($n = 10, 10, 10$ mice). **f**, Representative paths (left) and total time (right) spent in the center zone of the arena in the open field test. **g**, Total time spent in the open arm of the elevated plus maze test ($n = 9, 10, 9$ mice). **h**, Total immobile time in the tail suspension test ($n = 10, 10, 10$ mice). **i**, Total immobile time in the forced swim test ($n = 10, 10, 10$ mice). In **b**, **c** and **f**, the representative traces of these experiments were obtained from at least 80% in the total tested mice. All data are shown as mean ± s.e.m. Statistical significance was assessed by unpaired Student's *t* test; $^{*}P < 0.05$; $^{**}P < 0.001$. For detailed numbers and statistical analysis, see Supplementary Table 3.

Fig. 5). We then measured the spatial memory of the mice using the Morris water maze task, which assesses the ability to use distal spatial cues to locate a submerged platform. Compared to the control mice, the pCaMKIIα-driving mice (*Syt1* deleted in glutamatergic neurons) showed longer latencies to locate the escape platform during the training days and spent less time on the platform and in the correspondent quadrant during the test (Fig. 4a,b). These observations indicated that pCaMKIIα mice had a resistance to the acquisition of learning and reference memory. In sharp contrast, the pVGAT-driving mice with *Syt1* deficiency exclusively in GABAergic neurons showed superior learning and memory competency during the whole Morris water maze test compared to controls (Fig. 4a,b). Similarly, in a Barnes maze test, we found that, compared to controls, pCaMKIIα mice took a longer time to find the target refuge during the acquisition phase and the new refuge during the probing trial, whereas the pVGAT mice took much shorter times (Fig. 4c). We also tested reward–long-delay learning using a T-maze test. The pCaMKIIα mice showed a lower rate of correct alternation of entry into the unbaited arm compared to controls, whereas pVGAT mice exhibited the opposite tendency (Fig. 4d). Hence, the results of the three spatial memory-related tests all indicated that the shift of the E-I balance toward excitation improved the animals' spatial discrimination capacity, whereas shifting toward inhibition decreased this ability. To further evaluate associative learning, we performed a fear-conditioning test. The results indicated that compared to controls, pCaMKIIα- and pVGAT-driving *Syt1* KD mice showed attenuation and enhancement, respectively, in freezing in response to the conditioned and cued stimulus (Fig. 4e). We therefore concluded that shifting the E-I equilibrium within the DG generated parallel, bidirectional regulation of spatial and contextual fear memories in the mice.

It has been suggested that acute manipulation of neuronal activity in the hippocampus can generate emotional changes[1,2]. We evaluated the chronic CRISPRi-based regulation of the E-I balance in the DG on the affective status of the mice. The results of open field and elevated plus maze tests, which are typically used to assess anxiety-like behaviors, revealed that both the pCaMKIIα- and pVGAT-driving *Syt1* KD mice spent less time in the center of the field and in the open arm of the maze compared to controls, exhibiting anxiety-like phenotypes (Fig. 4f,g). Furthermore, in the tail suspension and forced swim tests, which can indicate the extent of depressive mood, both pCaMKIIα- and pVGAT-driving *Syt1* KD mice showed increased immobile times (Fig. 4h,i), indicating that both types of mice were subject to depression-like behaviors. Together, our results indicated that an aberrant E-I equilibrium within the DG, in either direction, dampened the mental status of the animals.

CRISPRi achieves multiplex gene silencing in the brain. Interrogation of the protein complex in the brain has been challenging, as inactivation of multiple functionally related genes usually requires laborious crossing of different inbred animal strains. Given the superior inhibition efficacy of the CRISPRi system, we sought to test whether CRISPRi could be used for multiplex gene silencing in the brain. To this end, we constructed an all-in-one lentiviral system, integrating dCas9-KRAB and two or three sgRNAs that were driven by different RNA polymerase III promoters into a single vector (Fig. 5a). In an alternative experiment, we constructed a dual-vector CRISPRi system that included one vector solely expressing the dCas9-KRAB and another vector encoding five U6::sgRNA cassettes assembled in a tandem array (Fig. 5a). Active sgRNAs targeting five genes, *Syt1*, *Vamp2*, *Snap25*, *Stx1a* and *Stx1b*, were employed to test

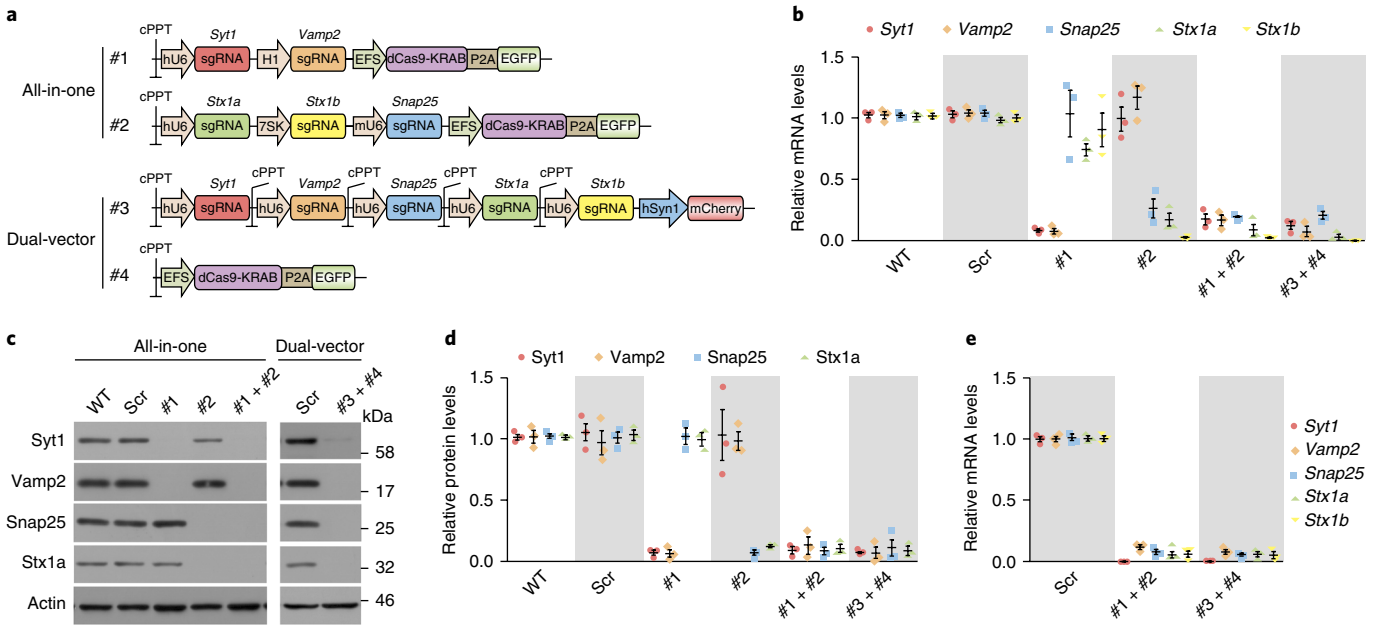

Fig. 5 | Flexible multiplex gene silencing using CRISPRi in the mouse brain. a, Schematic illustration of the all-in-one and dual-vector strategies for multigene targeting CRISPRi. cPPT, central polypurine tract. **b**, qRT-PCR analysis of mRNA expression of primary neurons infected with multiplex gene targeting CRISPRi lentivirus. **c**,**d**, Immunoblot analysis (**c**) and quantification (**d**) of protein expression in neurons expressing multiplex gene targeting CRISPRi. In **c**, blots are cropped; full-length blots are presented in Supplementary Fig. 8. **e**, qRT-PCR analysis of mRNA expression in neurons expressing multiplex CRISPRi in the mouse brain. In **b**–**e**, #1–4 are as in **a**. For all experiments, horizontal bars are the means of three independent biological replicates with similar results. Unpaired Student's *t* test; error bars show s.e.m. For detailed numbers and statistical analysis, see Supplementary Table 3.

the efficiency of these two multiplex strategies. We found that in the cultured hippocampal neurons, both the all-in-one and dual-vector systems efficiently abolished the mRNA and protein expression of the target two to five genes (Fig. 5b–d), with an efficacy comparable to that of single gene inactivation (Fig. 1b–d). Moreover, the all-in-one system could be combinatorially applied to achieve efficient silencing of a larger number of genes. We then stereotactically infused the lentiviruses encoding the combinatorial all-in-one system or the dual-vector system into the DG of adult mice. After 2 weeks, the infected neurons were purified as described (Fig. 3c). qRT-PCR analysis revealed that the mRNA expression of these genes was abolished (Fig. 5e), which is consistent with our observations in primary neurons. Taken together, our results demonstrate that CRISPRi can achieve highly efficient multiplex gene silencing in the brain.

Discussion

In this study, we developed a CRISPRi-based KD approach for rapid, convenient and specific gene inactivation in the brain. Our data showed that CRISPRi suppressed gene function efficiently and homogeneously in neurons. Notably, dCas9-based CRISPRi showed superior targeting specificity, with minimal off-target effects. To enrich the CRISPR toolbox, we engineered conditional CRISPRi tools to selectively inactivate genes in different subtypes of neurons. Using this toolbox, we modulated the E-I balance within the DG of mice and demonstrated that the DG regulates learning and mood processes in distinct patterns. Finally, we developed two multiplex KD strategies and achieved highly efficient abolishment of multiple genes encoding a protein complex crucial for brain functioning.

Efficient maneuverability of gene suppression by CRISPRi. CRISPR–Cas9 has high genome-editing efficiency compared to other programmable gene-editing systems and thus is suitable for the construction of knockout animal strains and cell lines[3–8]. Although there might be off-target DNA cleavage and divergent indels that might generate differential genotypes, ideal gene-edited candidates can often be selected out for follow-up studies. However, as postmitotic neurons cannot establish homologous gene-modified cell lines, cleavage by CRISPR–Cas9 could result in mosaic and unpredictable targeted gene mutations in these cells. Hence, gene editing in the brain has very strict requirements for global efficiency and homogeneity. In the present study, we used dCas9 as a carrier to transport a well-defined transcription repressor (KRAB) to the target locus of the neuronal genome[18,19], thus indirectly silencing the gene through this repressor. Our results indicated that the efficiency of CRISPRi in postmitotic neurons was superior to the RNAi technique. Compared to conventional CRISPR–Cas9 technology, on the one hand, this approach would not generate genotypic mosaic, because dCas9 does not alter the chromosomal DNA sequence[9]; on the other hand, as transcription of genes is always initiated from the TSS region, sgRNAs would be more likely to bind to the TSS region than to access exons and introns, which would increase the inactivation efficiency.

Our study also indicated that this approach has additional advantages that enhance its application in neurons. First, dCas9-KRAB showed low tolerance for even slight mispairings between the sgRNA and the target locus, and thus the off-target DNA binding activity was very weak. As the DNA-association threshold for dCas9-KRAB to produce inhibitory effects is very high, the residual DNA binding activity of dCas9-KRAB detected in our ChIP-based experiments was insufficient to affect normal gene expression. Second, a gene rescue or mutation study could be done simply by introducing the exogenous wild-type or mutated gene with a different promoter. Compared to the rescue of CRISPR–Cas9-induced gene cleavage or RNAi in an almost mandatory locus-mutated way, CRISPRi is obviously more convenient.

All these merits guarantee that dCas9-KRAB-mediated KD possesses superior gene-silencing efficacy, negligible deflected targeting activity and efficient maneuverability in neural study. We therefore conclude that the dCas9-KRAB-based CRISPRi approach is an effective solution for gene inactivation in the brain.

Versatile application of a dCas9-based CRISPR toolbox for rapid gene modification in the brain. Current research in the brain usually requires neuronal subtype-specific and brain region-specific modification of genes. Using CRISPRi, we can achieve these goals in a rapid and convenient way. In this study, we verified the efficiency and specificity of the conditional glutamatergic and GABAergic CRISPRi systems in the mouse hippocampus using molecular, electrophysiological and behavioral testing approaches, thus proving that dCas9-based technology has wide prospects for research in the brain. First, CRISPRi can be expanded to a list of neuronal subtypes such as dopaminergic, serotoninergic and GABAergic parvalbumin- or somatostatin-expressing neurons, which are known to be involved in the etiology of a number of neuropsychiatric and neurodegenerative disorders[36–39]. Second, the high efficiency of multiplex gene KD by CRISPRi may facilitate understanding the relationship of proteins within a complex or signaling pathway in the brain. Interference with a single gene in a network may not only inadequately disturb the biological process of interest but may also make it more difficult to determine the more salient of genes that are functionally redundant. Leveraging the advantage of CRISPRi, we were able to silence five genes in vivo. We therefore believe that multiplex CRISPRi can enhance the interrogation of complex protein machinery and multigenic neuronal disorders, which so far have remained serious challenges. Third, in addition to CRISPR-based interference, CRISPR technology can be engineered to be a flexible and versatile tool for neurobiology. It has been suggested that the synergistic activation mediator system[40], in which VP64 is conjugated to dCas9 in combination with p65 and HSF1, can upregulate the expression of endogenous genes. Indeed, in the present study, we found that the synergistic activation mediator system targeting the endogenous *Syt1* gene substantially enhanced the expression of Syt1 protein and mRNA (Supplementary Fig. 6). In the future, it will be worthwhile to further supplement the dCas9-based toolbox to achieve divergent research goals in the brain.

In addition to the merits of CRISPRi technology in brain research, our study indicated that neuronal models can be a suitable platform for investigating the mechanisms of CRISPR–Cas9. Previously, thoughtful insights into the specificity and mechanism of the Cas9–sgRNA complex have been gained largely based on in vitro reconstitution systems or fast-dividing cell lines[9,28,41–43]. As Cas9-involved events are transient in proliferative cells, high-affinity dCas9 and high-cost genome sequencing approaches are often used to evaluate Cas9–sgRNA–DNA interactions[44–48]. On the one hand, it has been suggested that dCas9 has distinctive biophysical characteristics compared to wild-type Cas9[41,45,49,50]; on the other hand, the cells could proliferate in an unbalanced manner, which would consequently affect data interpretation. Therefore, a nondividing cell model in which the Cas9–chromatin interaction events could be retained for a relatively long period seemed appropriate for precise investigation of Cas9 or dCas9 functioning and specificity in vivo. In the present study, using cultured neurons as a platform, we were able to monitor dCas9 functioning in a 14-d time window. In the future, it will be interesting to detect and analyze active and transient CRISPR–chromatin interactions in quiescent neurons.

Conclusions

Our results demonstrate that CRISPRi enables fast and accurate gene function readouts in neurons in vivo and in vitro. The dCas9-based CRISPR toolbox will complement neurophysiological and optogenetic dissection of gene function in divergent populations of neurons.

Methods

Methods, including statements of data availability and any associated accession codes and references, are available at https://doi.org/10.1038/s41593-018-0077-5.

Received: 17 January 2017; Accepted: 28 December 2017;
Published online: 5 February 2018

References

1. Kheirbek, M. A. et al. Differential control of learning and anxiety along the dorsoventral axis of the dentate gyrus. *Neuron* **77**, 955–968 (2013).
2. Ramirez, S. et al. Activating positive memory engrams suppresses depression-like behaviour. *Nature* **522**, 335–339 (2015).
3. Chen, Y. et al. Engineering human stem cell lines with inducible gene knockout using CRISPR/Cas9. *Cell. Stem Cell.* **17**, 233–244 (2015).
4. Bauer, D. E., Canver, M. C. & Orkin, S. H. Generation of genomic deletions in mammalian cell lines via CRISPR/Cas9. *J. Vis. Exp.* **95**, e52118 (2015).
5. Merkle, F. T. et al. Efficient CRISPR-Cas9-mediated generation of knockin human pluripotent stem cells lacking undesired mutations at the targeted locus. *Cell Rep.* **11**, 875–883 (2015).
6. Yang, H. et al. One-step generation of mice carrying reporter and conditional alleles by CRISPR/Cas-mediated genome engineering. *Cell* **154**, 1370–1379 (2013).
7. Wang, H. et al. One-step generation of mice carrying mutations in multiple genes by CRISPR/Cas-mediated genome engineering. *Cell* **153**, 910–918 (2013).
8. Platt, R. J. et al. CRISPR-Cas9 knockin mice for genome editing and cancer modeling. *Cell* **159**, 440–455 (2014).
9. Jinek, M. et al. A programmable dual-RNA-guided DNA endonuclease in adaptive bacterial immunity. *Science* **337**, 816–821 (2012).
10. Cong, L. et al. Multiplex genome engineering using CRISPR/Cas systems. *Science* **339**, 819–823 (2013).
11. Mali, P. et al. RNA-guided human genome engineering via Cas9. *Science* **339**, 823–826 (2013).
12. Incontro, S., Asensio, C. S., Edwards, R. H. & Nicoll, R. A. Efficient, complete deletion of synaptic proteins using CRISPR. *Neuron* **83**, 1051–1057 (2014).
13. Straub, C., Granger, A. J., Saulnier, J. L. & Sabatini, B. L. CRISPR/Cas9-mediated gene knock-down in post-mitotic neurons. *PLoS One* **9**, e105584 (2014).
14. Swiech, L. et al. In vivo interrogation of gene function in the mammalian brain using CRISPR-Cas9. *Nat. Biotechnol.* **33**, 102–106 (2015).
15. Dominguez, A. A., Lim, W. A. & Qi, L. S. Beyond editing: repurposing CRISPR-Cas9 for precision genome regulation and interrogation. *Nat. Rev. Mol. Cell. Biol.* **17**, 5–15 (2016).
16. Ma, H. et al. Multiplexed labeling of genomic loci with dCas9 and engineered sgRNAs using CRISPRainbow. *Nat. Biotechnol.* **34**, 528–530 (2016).
17. Nelles, D. A. et al. Programmable RNA tracking in live cells with CRISPR/Cas9. *Cell* **165**, 488–496 (2016).
18. Gilbert, L. A. et al. Genome-scale CRISPR-mediated control of gene repression and activation. *Cell* **159**, 647–661 (2014).
19. Gilbert, L. A. et al. CRISPR-mediated modular RNA-guided regulation of transcription in eukaryotes. *Cell* **154**, 442–451 (2013).
20. Fulco, C. P. et al. Systematic mapping of functional enhancer-promoter connections with CRISPR interference. *Science* **354**, 769–773 (2016).
21. Adamson, B. et al. A multiplexed single-cell CRISPR screening platform enables systematic dissection of the unfolded protein response. *Cell* **167**, 1867–1882.e21 (2016).
22. Thakore, P. I. et al. Highly specific epigenome editing by CRISPR-Cas9 repressors for silencing of distal regulatory elements. *Nat. Methods* **12**, 1143–1149 (2015).
23. Liu, S. J. et al. CRISPRi-based genome-scale identification of functional long noncoding RNA loci in human cells. *Science* **355**, eaah7111 (2017).
24. Shalem, O. et al. Genome-scale CRISPR-Cas9 knockout screening in human cells. *Science* **343**, 84–87 (2014).
25. Söllner, T. et al. SNAP receptors implicated in vesicle targeting and fusion. *Nature* **362**, 318–324 (1993).
26. Südhof, T. C. & Rothman, J. E. Membrane fusion: grappling with SNARE and SM proteins. *Science* **323**, 474–477 (2009).
27. Geppert, M. et al. Synaptotagmin I: a major $Ca2^{+}$ sensor for transmitter release at a central synapse. *Cell* **79**, 717–727 (1994).
28. Hsu, P. D. et al. DNA targeting specificity of RNA-guided Cas9 nucleases. *Nat. Biotechnol.* **31**, 827–832 (2013).
29. Root, D. E., Hacohen, N., Hahn, W. C., Lander, E. S. & Sabatini, D. M. Genome-scale loss-of-function screening with a lentiviral RNAi library. *Nat. Methods* **3**, 715–719 (2006).
30. Groffen, A. J. et al. Doc2b is a high-affinity Ca2+ sensor for spontaneous neurotransmitter release. *Science* **327**, 1614–1618 (2010).
31. Yao, J., Gaffaney, J. D., Kwon, S. E. & Chapman, E. R. Doc2 is a Ca2+ sensor required for asynchronous neurotransmitter release. *Cell* **147**, 666–677 (2011).
32. Dittgen, T. et al. Lentivirus-based genetic manipulations of cortical neurons and their optical and electrophysiological monitoring in vivo. *Proc. Natl. Acad. Sci. USA* **101**, 18206–18211 (2004).

33. Oh, W. J., Noggle, S. A., Maddox, D. M. & Condie, B. G. The mouse vesicular inhibitory amino acid transporter gene: expression during embryogenesis, analysis of its core promoter in neural stem cells and a reconsideration of its alternate splicing. *Gene* **351**, 39–49 (2005).
34. Kerr, A. M., Reisinger, E. & Jonas, P. Differential dependence of phasic transmitter release on synaptotagmin 1 at GABAergic and glutamatergic hippocampal synapses. *Proc. Natl. Acad. Sci. USA* **105**, 15581–15586 (2008).
35. Jackman, S. L. & Regehr, W. G. The mechanisms and functions of synaptic facilitation. *Neuron* **94**, 447–464 (2017).
36. Deneris, E. S. & Wyler, S. C. Serotonergic transcriptional networks and potential importance to mental health. *Nat. Neurosci.* **15**, 519–527 (2012).
37. Pehrson, A. L. & Sanchez, C. Altered γ-aminobutyric acid neurotransmission in major depressive disorder: a critical review of the supporting evidence and the influence of serotonergic antidepressants. *Drug. Des. Devel. Ther.* **9**, 603–624 (2015).
38. Perez, S. M. & Lodge, D. J. Hippocampal interneuron transplants reverse aberrant dopamine system function and behavior in a rodent model of schizophrenia. *Mol. Psychiatry* **18**, 1193–1198 (2013).
39. Lewis, D. A., Hashimoto, T. & Volk, D. W. Cortical inhibitory neurons and schizophrenia. *Nat. Rev. Neurosci.* **6**, 312–324 (2005).
40. Konermann, S. et al. Genome-scale transcriptional activation by an engineered CRISPR-Cas9 complex. *Nature* **517**, 583–588 (2015).
41. Sternberg, S. H., Redding, S., Jinek, M., Greene, E. C. & Doudna, J. A. DNA interrogation by the CRISPR RNA-guided endonuclease Cas9. *Nature* **507**, 62–67 (2014).
42. Szczelkun, M. D. et al. Direct observation of R-loop formation by single RNA-guided Cas9 and Cascade effector complexes. *Proc. Natl. Acad. Sci. USA* **111**, 9798–9803 (2014).
43. Lin, Y. et al. CRISPR/Cas9 systems have off-target activity with insertions or deletions between target DNA and guide RNA sequences. *Nucleic Acids Res.* **42**, 7473–7485 (2014).
44. Wu, X. et al. Genome-wide binding of the CRISPR endonuclease Cas9 in mammalian cells. *Nat. Biotechnol.* **32**, 670–676 (2014).
45. Kuscu, C., Arslan, S., Singh, R., Thorpe, J. & Adli, M. Genome-wide analysis reveals characteristics of off-target sites bound by the Cas9 endonuclease. *Nat. Biotechnol.* **32**, 677–683 (2014).
46. O'Geen, H., Henry, I. M., Bhakta, M. S., Meckler, J. F. & Segal, D. J. A genome-wide analysis of Cas9 binding specificity using ChIP-seq and targeted sequence capture. *Nucleic Acids Res.* **43**, 3389–3404 (2015).
47. Cencic, R. et al. Protospacer adjacent motif (PAM)-distal sequences engage CRISPR Cas9 DNA target cleavage. *PLoS. One* **9**, e109213 (2014).
48. Duan, J. et al. Genome-wide identification of CRISPR/Cas9 off-targets in human genome. *Cell. Res.* **24**, 1009–1012 (2014).
49. Knight, S. C. et al. Dynamics of CRISPR-Cas9 genome interrogation in living cells. *Science* **350**, 823–826 (2015).
50. Tsai, S. Q. et al. GUIDE-seq enables genome-wide profiling of off-target cleavage by CRISPR-Cas nucleases. *Nat. Biotechnol.* **33**, 187–197 (2015).

Acknowledgements

We thank P.D. Hsu (The Salk Institute for Biological Studies, USA) and S. Shi (Memorial Sloan Kettering Cancer Center, USA) for discussion and comments. We thank J. Guan (Tsinghua University, China) for material help. We also thank all members of the Yao laboratory for assistance. This work was supported by the National Key R&D Program of China (Grant No. 2016YFA0101900, 2016YFC0903301), National Natural Science Foundation of China (Grant No. 31771482, 31471020, 31161120358), National Basic Research Program of China (Grant No. 2015CB910603), Beijing Municipal Science & Technology Commission (Grant No.Z161100002616010), the Key Research Program of the CAS (Grant No. KJZD-EW-L14), the Open Project of Key Laboratory of Genomic and Precision Medicine of the CAS, the Open Project of State Key Laboratory of Membrane Biology of China, The JPB Foundation, The Leona M. and Harry B. Helmsley Charitable Trust, Annette C. Merle-Smith, NIH grants R01MH114030 (F.H.G) and NIH U19MH106434 (F.H.G), and The G. Harold & Leila Y. Mathers Foundation.

Author contributions

J.Y. and F.H.G. conceived the project. J.Y. and S.M. designed the experiments. Y.Z., Y.-N.L., J.Z., Y.-Z.X. and S.M. conducted ChIP experiments. Y.Z., Y.-N.L. and X.Y. conducted western blotting, qPCR and molecular biology experiments. H.Q. and B.Y. performed electrophysiological experiments and analyzed data. W.S., Y.Z., Y.C., S.-Y.L. and Y.L. conducted stereotactic infusion and immunofluorescence experiments. W.S. conducted animal behavioral experiments and analyzed data. Y.Z. and J.Y. analyzed experimental results and wrote the manuscript with input from all authors.

Competing interests

The authors declare no competing financial interests.

Additional information

Supplementary information accompanies this paper at https://doi.org/10.1038/s41593-018-0077-5.

Reprints and permissions information is available at www.nature.com/reprints.

Correspondence and requests for materials should be addressed to S.M. or J.Y.

Publisher's note: Springer Nature remains neutral with regard to jurisdictional claims in published maps and institutional affiliations.

Methods

Plasmid construction and sgRNA design. The lentiviral vector used for this study was modified from the lentiCRISPR v2 vector (#52961) obtained from Addgene, with the puromycin cassette replaced by EGFP. Hence, the EGFP protein was simultaneously expressed with Cas9 via a self-cleaving 2 A peptide (P2A). dCas9 was generated by replacing the Asp10 and His840 residues of Cas9 with alanine. For KD, a KRAB transcription repressor was conjugated to the N-terminus of dCas9. The TSS was identified using the FANTOM5/CAGE promoter atlas[51,52]. The sgRNAs were designed to target the DNA region from −50 to 300 bp relative to the TSS of the candidate genes[18], using the web tool http://crispr.mit.edu/ to minimize the off-target effect[28] (Supplementary Table 1). The two sgRNAs with the highest scores were designed for each tested genes. For the selective expression of dCas9-KRAB, the EFS promoter was replaced by the mouse pCaMKIIα or pVGAT promoter[32,33]. For multiplex gene targeting, individual sgRNA cassettes were assembled using the Golden Gate cloning strategy. The shRNAs used in this study were purchased from The RNAi Consortium (TRC) library (https://www.broadinstitute.org/rnai-consortium/rnai-consortium-shrna-library).

Cell culture, lentivirus production and transfection. Hippocampal neurons were dissected from postnatal day 1 (P1) C57BL/6 pups. After removal of the meninges, the hippocampi were minced and incubated for 15 min in 0.25% trypsin (Life Technologies) at 37 °C. After washing, the neurons were mechanically triturated and cultured in Neurobasal-A medium (Life Technologies) supplemented with 2% B-27 (Life Technologies) and 2 mM Glutamax (Life Technologies). For cortical neurons, digestion was carried out using 0.2% trypsin for 10 min at 37 °C. Primary cultures were maintained in a humidified 5% CO_2 incubator at 37 °C. Primary neurons were infected with lentivirus at 3 DIV and subjected to experiments at 14–17 DIV. We typically used a multiplicity of infection (MOI) of 10 in primary cultures. For rescue experiments, lentivirus encoding the rescue exogenous gene was applied at 5 DIV. For the dual-vector multiplex experiments, neurons were first infected with lentivirus expressing dCas9-KRAB at 3 DIV and then infected with the sgRNA-encoding lentivirus at 5 DIV.

HEK293FT cells were maintained in Dulbecco's modified eagle medium (DMEM) in 10% FBS, 100 units/mL streptomycin and 100 mg/mL penicillin with 2 mM Glutamax (Life Technologies). Lentiviral particles were generated by cotransfecting HEK293FT cells with virus packaging vectors (pVSVg and psPAX2). Transfection was performed using PEI (Polysciences). Five hours after transfection, the medium was changed. Virus supernatant was harvested 60 h post-transfection, filtered with a 0.22-μm PVDF filter (Millipore), ultracentrifuged at 25,000 rpm using a P28S rotor (Hitachi) and stocked in a final volume of 100 μL. The titer of the lentivirus used in all cell culture experiments was at least 5.0×10^8 infectious units (IU) per ml. For in vivo stereotactic infusion experiments, the lentivirus was further concentrated to a titer of 1.0×10^{10} IU/mL, and different multiplex CRISPRi viruses were mixed in equal amounts before infusion.

Lentivirus infusion. Following anesthesia with a mixture of oxygen and isoflurane, 4-week-old C57BL/6 male mice were stereotactically infused with lentivirus encoding dCas9-KRAB and either targeting or scramble sgRNA. The lentivirus was infused bilaterally into the hippocampal DG region at coordinates AP −2.0 mm, ML ±1.5 mm and DV −2.5 mm relative to bregma. Viral solution (1.0×10^{10} IU/mL, 1 μL) in a glass cannula was infused using a microinjection pump (Harvard Apparatus) at a flow rate of 0.1 μL/min into each hemisphere sequentially. The mice were subjected to behavioral, immunohistochemical or flow cytometric analysis tests after 2 weeks.

Immunoblot analysis. Primary neurons were lysed in RIPA buffer (50 mM Tris-Cl, pH 8.0, 150 mM NaCl, 1% Nonidet P-40, 0.5% sodium deoxycholate and 0.1% SDS) plus a complete protease inhibitor cocktail (Roche). Lysates were centrifuged and supernatants were subjected to SDS-PAGE. Primary antibodies were as follows: rabbit polyclonal anti-synaptotagmin 1 antibody (1:2,000, Abcam, #ab131551), rabbit polyclonal anti-VAMP2 antibody (1:2,000, Abcam, #ab3347), mouse monoclonal anti-SNAP25 antibody (1:5,000, Synaptic Systems, #111011), mouse monoclonal anti-syntaxin-1a antibody (1:2,000, Synaptic Systems, #110111) and mouse monoclonal anti-actin antibody (1:5,000, Abcam, #ab6276). The blots were developed using an ECL kit (Pierce). Protein levels were quantified by densitometry using the NIH ImageJ 1.48 software (https://rsb.info.nih.gov/ij/).

Immunofluorescence. For immunostaining of the neuronal culture, neurons were fixed in 4% paraformaldehyde and then permeabilized with 0.3% Triton X-100. After blocking with 5% goat serum and 0.1% Triton X-100, cells were incubated with appropriate primary antibodies overnight at 4 °C. After washing, cells were incubated with secondary antibodies for 1 h at room temperature (23–25 °C). For immunostaining of brain slices, mice were killed for analysis 2 weeks after viral delivery and transcardially perfused with 4% PFA in PBS. Fixed tissue was sectioned at 50 μm thickness using a vibratome (Leica, VT1000S). Next, antigens were retrieved by incubating for 10 min in 100 mM Tris (pH 7.4). Sections were blocked with 5% normal goat serum (NGS) in TBST (137 mM NaCl, 20 mM Tris, pH 7.6, 0.05% Tween-20) for 1 h and incubated with primary antibodies overnight at 4 °C. After three washes in TBST, samples were incubated with secondary antibodies. Fluorescent signals were detected on an Olympus FV1200 confocal microscope by sequential acquisition or on slide scanner (Zeiss, Axio Scan.Z1) and images were processed using ImageJ 1.48 software.

Primary antibodies were as follows: chicken polyclonal anti-GFP antibody (1:1,000, Abcam, #ab13970), rabbit polyclonal anti-GABA antibody (1:1,000, Calbiochem, #PC213L), rabbit polyclonal anti-VGLUT1 antibody (1:500, Abcam, #ab104898) and rabbit polyclonal anti-synaptotagmin-1 antibody (1:100, Abcam, #ab131551). Secondary antibodies were donkey anti-chicken Alexa Fluor-488 antibody (1:1,000, Jackson ImmunoResearch, #703-545-155) and donkey anti-rabbit Cy3 antibody (1:1,000, Jackson ImmunoResearch, #711-165-152).

Quantitative reverse-transcription PCR. Total RNA was isolated using Trizol (Life Technologies) according to the manufacturer's instructions. cDNA was synthesized using SuperScript III Reverse Transcription Kit (Life Technologies), and quantitative reverse-transcription PCR (qRT-PCR) was performed on a Bio-Rad CFX96 thermal cycler using SYBR green supermix (Bio-Rad) and gene-specific primers (Supplementary Table 2). Quantitative analysis was performed employing the ΔΔCT method and using *Gapdh* as the endogenous control.

Chromatin immunoprecipitation. To crosslink protein–DNA complexes, formaldehyde (Sigma) was added at a final concentration of 1% and rotated gently at room temperature for 10 min. Crosslinking was quenched by adding 125 mM glycine for 5 min at room temperature. After washing, cells were lysed in 0.5 mL cold lysis buffer (50 mM HEPES-KOH, pH 7.5, 140 mM NaCl, 1 mM EDTA, 10% glycerol, 0.5% Nonidet P-40, 0.25% Triton X-100 and complete protease inhibitor cocktail) for 10 min at 4 °C. The lysate was then pelleted and the sedimented nuclei were resuspended in 0.2 mL sonication buffer (50 mM Tris-Cl, pH 8.1, 10 mM EDTA, 1% SDS and complete protease inhibitor cocktail) and sonicated (5 min total time, 30 s on, 30 s off, set at 20% amplitude) in an ultrasonic processor (Sonics and Materials) to shear the DNA into 200- to 2,000-bp fragments. The supernatant was diluted and precleared by adding 20 μL prerinsed Protein A/G Agarose (Santa Cruz Biotechnology) and incubated for 1 h at 4 °C. After preclearing, 50 μL supernatant was saved as input control. The remaining lysate was incubated overnight at 4 °C with 5 μg monoclonal anti-FLAG M2 antibody (Sigma, #F1804) or purified mouse IgG1 isotype control antibody (BD Pharmingen, #550878) for immunoprecipitation. The next day, 50 μL Protein G Dynabeads were added to each ChIP reaction and the result was further incubated for 1 h at 4 °C. After washing, the purified material was eluted from the beads twice with 50 μL elution buffer (0.1 M $NaHCO_3$ and 1% SDS) by violently vortexing for 15 min at room temperature. The eluents and inputs added at a final concentration of 200 mM NaCl were reverse-crosslinked by boiling for 15 min. The resulting genomic DNA fragments were then purified using a QIAquick PCR Purification Kit (Qiagen) following the manufacturer's instructions. Samples were assessed for enrichment by qPCR.

Electrophysiology. Whole-cell recordings were performed in voltage-clamp mode using a MultiClamp 700B amplifier (Molecular Devices). The recording chamber was continuously perfused with a bath solution (128 mM NaCl, 30 mM glucose, 5 mM KCl, 5 mM $CaCl_2$, 1 mM $MgCl_2$, and 25 mM HEPES; pH 7.3) at room temperature. Patch pipettes were pulled from borosilicate glass and had resistances of 4–7 MΩ. For the EPSC recordings, 50 μM D-AP5 (NMDA receptor antagonist, Tocris) and 20 μM bicuculline ($GABA_A$ receptor antagonist, Tocris) were applied to isolate AMPA receptor-mediated EPSCs, and pipettes were filled with internal solution containing 125 mM potassium gluconate, 10 mM KCl, 5 mM EGTA, 10 mM HEPES, 10 mM Tris-phosphocreatine, 4 mM Mg-ATP, 0.5 mM Na_2GTP and 5 mM QX-314; pH 7.3. For the IPSC recordings, 50 μM D-AP5 and 20 μM CNQX (Sigma) were applied to the bath solution, and patch pipettes were filled with internal solution containing 147 mM CsCl, 5 mM Tris-phosphocreatine, 2 mM EGTA, 10 mM HEPES, 2 mM MgATP, 0.3 mM Na_2GTP and 5 mM QX-314; pH 7.3. The series resistance of the pipettes was typically <15 MΩ and was partially compensated to 60–80%. The membrane potential was held at −70 mV. To trigger an action potential, we depolarized presynaptic neurons with a theta-stimulating electrode and a voltage step from 0 V to 20–30 V for 1 ms; EPSCs or IPSCs were recorded from connected postsynaptic neurons. Data were acquired and analyzed using pClamp 10 software (Molecular Devices), sampled at 10 kHz and filtered at 2 kHz. Data are presented as mean ± s.e.m.

Fluorescence activated cell sorting. Two weeks after viral delivery, adult male mice were perfused in perfusion buffer (115 mM choline-chloride, 2.5 mM KCl, 1.25 mM NaH_2PO_4, 26 mM $NaHCO_3$, 10 mM D-(+)-glucose, 8 mM $MgSO_4$, 1 mM L-ascorbate-Na, 3 mM Na-pyruvate; pH 7.2–7.4) and decapitated, and the brain was quickly removed and sectioned on a vibratome on ice. Individual slices of interest were transferred to a small petri dish containing EBSS buffer (116 mM NaCl, 5.4 mM KCl, 26 mM $NaHCO_3$, 1 mM NaH_2PO_4, 1.5 mM $CaCl_2$, 1 mM $MgSO_4$, 0.5 mM EDTA, 25 mM glucose, 1 mM cysteine), bubbled with a carbogen gas (95% O_2 and 5% CO_2). The DG was microdissected and treated with carbogen-bubbled EBSS with 20 units/mL papain (Sigma) and 0.005% DNase I for 1 h at 37 °C. Digestion was terminated by EBSS buffer containing 1 mg/mL ovomucoid, 1 mg/mL BSA, and 0.005% DNase I in EBSS. The tissue pieces were dissociated

into single cells by gentle trituration. DAPI (2 ng/mL) was added to the single cell suspension to exclude dead cells.

Sorting was performed on a Beckman FACS sorter in the single-cell sorting mode using a 130-μm nozzle and sheath pressure of 10 psi. FACS populations were chosen to select cells with low DAPI and high EGFP fluorescence. cDNA was amplified according to the Smart-seq2 protocol[53]. Primary cultured cortical neurons infected with EGFP-expressing lentivirus were trypsinized, terminated with 10% FBS, filtered through a 200-mesh cell sieve and subjected to sorting $EGFP^+$ and $EGFP^-$ cells simultaneously.

Behavioral methods. All the animal experiments were conducted under the guidance and approval of the Institutional Animal Care & Use Committee of Tsinghua University and the Animal Welfare and Ethics Committee of Tsinghua University (Approval ID: 15-YJ2). Mice were maintained in a 12-h light/12-h dark cycle with a maximum of five animals per cage and with standard mouse chow and water ad libitum. Behavioral tests were performed during the light phase in the second half of the day. All behavioral tests except for the Morris water maze test were conducted in the same group of animals. Following behavioral tests, animals were dissected to perform immunostaining analysis to verify virus infection, and animals without appropriate lentivirus infection were excluded from analysis. Animals that accidentally died during the study were included in analysis for all completed tests. The data were analyzed by EthoVision XT 11.5 software (Noldus).

Morris water maze test. A circular tank (1.2-m diameter) was filled with water (24 °C, 30 cm deep). The walls surrounding the tank were decorated with bright, contrasting shapes that served as reference cues. The escape platform (6 cm in diameter) was kept in a fixed quadrant. Four trials per day were conducted with intervals of 40 min for 8 d. Mice were allowed to search for a platform for 60 s or were guided to it for 10 s if they did not find a platform. After reaching the platform, the animal was allowed to stay for 10 s before being removed from the tank. On day 9 of the experiment, the platform was removed and a memory test was conducted for 1 min. The time spent on the platform and in each quadrant was analyzed.

Fear conditioning test. On the training day, mice were habituated to the conditioning chamber for 6 min and then experienced two pairings of a tone (2,800 Hz, 75 dB, 20 s) with a co-terminating foot shock (0.7 mA, 2 s) at 3 min intervals. On test day 1, each mouse was returned to the chamber for 6 min without the tone. On test day 2, the mouse was returned to the chamber with a new context. After being habituated to the new context for 6 min, they were exposed to two 20-s tones with 3-min intervals. Freezing was defined as being motionless. The amount of time spent freezing was expressed as a percentage of total session time.

T maze test. Mice were food-restricted (2 g feed/mouse) to 85% of free-feeding body weight until the task was completed. Mice were allowed to freely explore the T maze for 5 min and eat the reward food (0.2 g chocolate, five times per day) for 2 d to become habituated to the apparatus. The test consisted of the training phase for 8 consecutive days and the testing phase on day 9. Mice were trained with one forced choice and one free choice at intervals of 20 s (the training phase) or 60 s (the testing phase), four trials per day.

Barnes maze test. Mice were allowed to freely explore the Barnes maze apparatus for 15 min and were rewarded with food (0.2 g chocolate) for the first two days to become habituated to the apparatus. The food-searching training procedure was repeated a total of 10 times for each mouse, followed by the food searching test, performed five times. In the following new-home test, the mice were released from an uncued home base that was 180° different from what was encountered during training, with five trials per mouse. The distance and time between the mice finding the food and carrying it to the refuge were recorded. All mice were maintained at 85% of their ad libitum feeding weight during the experiment.

Open field test. An open field arena (50 cm × 50 cm × 40 cm) was used to measure animal locomotor activity. Mice were placed in the center of the arena and allowed to freely explore it for 10 min.

Elevated plus maze test. Mice were placed at the junction of the open and closed arms of the homemade maze, facing the open arm opposite the experimenter, and left to explore the maze for 5 min. The total time spent in open arms was recorded.

Tail suspension test. Mice were suspended above a solid surface by their tails with tape for 6 min. The duration of immobility was measured.

Forced swim test. Mice were put into cylindrical tanks that were filled with tap water set at room temperature (23–25 °C) for 6 min. Movements were recorded and immobile time was measured.

Statistical analysis. Data are presented as mean ± s.e.m. of the values from at least three independent experiments. Statistical significance was evaluated using two-tailed unpaired Student's *t* test at $P < 0.05$. Data distribution was assumed to be normal, but this was not formally tested. No statistical methods were used to predetermine sample sizes, but our sample sizes are similar to those reported in previous publications[14,18]. The experiments were not randomized and the investigators were not blinded to allocation during experiments and outcome assessment.

Life Sciences Reporting Summary. Further information on experimental design is available in the Life Sciences Reporting Summary.

Data availability. The data that support the findings of this study are available from the corresponding author upon reasonable request.

References

51. Radzisheuskaya, A., Shlyueva, D., Müller, I. & Helin, K. Optimizing sgRNA position markedly improves the efficiency of CRISPR/dCas9-mediated transcriptional repression. *Nucleic Acids Res.* **44**, e141 (2016).
52. Forrest, A. R. et al. A promoter-level mammalian expression atlas. *Nature* **507**, 462–470 (2014).
53. Picelli, S. et al. Full-length RNA-seq from single cells using Smart-seq2. *Nat. Protoc.* **9**, 171–181 (2014).

nature research

Corresponding author(s): Jun Yao

☐ Initial submission ☐ Revised version ☒ Final submission

Life Sciences Reporting Summary

Nature Research wishes to improve the reproducibility of the work that we publish. This form is intended for publication with all accepted life science papers and provides structure for consistency and transparency in reporting. Every life science submission will use this form; some list items might not apply to an individual manuscript, but all fields must be completed for clarity.

For further information on the points included in this form, see Reporting Life Sciences Research. For further information on Nature Research policies, including our data availability policy, see Authors & Referees and the Editorial Policy Checklist.

Experimental design

1. Sample size

Describe how sample size was determined.

No statistical methods were used to predetermine sample sizes, but our sample sizes are similar to those reported in previous publications.

2. Data exclusions

Describe any data exclusions.

In the "Behavioral methods" section of the "METHODS" part, we stated that animals without appropriate lentivirus infection were excluded from analysis.

3. Replication

Describe whether the experimental findings were reliably reproduced.

All attempts at replication were successful.

4. Randomization

Describe how samples/organisms/participants were allocated into experimental groups.

The experiments were not randomized.

5. Blinding

Describe whether the investigators were blinded to group allocation during data collection and/or analysis.

The investigators were not blinded to allocation during experiments and outcome assessment.

Note: all studies involving animals and/or human research participants must disclose whether blinding and randomization were used.

6. Statistical parameters

For all figures and tables that use statistical methods, confirm that the following items are present in relevant figure legends (or in the Methods section if additional space is needed).

n/a	Confirmed	
☐	☒	The exact sample size (*n*) for each experimental group/condition, given as a discrete number and unit of measurement (animals, litters, cultures, etc.)
☐	☒	A description of how samples were collected, noting whether measurements were taken from distinct samples or whether the same sample was measured repeatedly
☐	☒	A statement indicating how many times each experiment was replicated
☐	☒	The statistical test(s) used and whether they are one- or two-sided (note: only common tests should be described solely by name; more complex techniques should be described in the Methods section)
☒	☐	A description of any assumptions or corrections, such as an adjustment for multiple comparisons
☐	☒	The test results (e.g. *P* values) given as exact values whenever possible and with confidence intervals noted
☐	☒	A clear description of statistics including central tendency (e.g. median, mean) and variation (e.g. standard deviation, interquartile range)
☐	☒	Clearly defined error bars

See the web collection on statistics for biologists for further resources and guidance.

Software

Policy information about availability of computer code

7. Software

Describe the software used to analyze the data in this study.	We used NIH ImageJ 1.48 software (http://rsb.info.nih.gov/ij/) for densitometry and image analysis. We used pClamp 10 software (Molecular Devices) for electrophysiology analysis and EthoVision XT 11.5 software (Noldus) for behavioral analysis; Prism (GraphPad, California, USA) for statistics.

For manuscripts utilizing custom algorithms or software that are central to the paper but not yet described in the published literature, software must be made available to editors and reviewers upon request. We strongly encourage code deposition in a community repository (e.g. GitHub). *Nature Methods* guidance for providing algorithms and software for publication provides further information on this topic.

Materials and reagents

Policy information about availability of materials

8. Materials availability

Indicate whether there are restrictions on availability of unique materials or if these materials are only available for distribution by a for-profit company.	No unique material were used.

9. Antibodies

Describe the antibodies used and how they were validated for use in the system under study (i.e. assay and species).	rabbit polyclonal anti-Synaptotagmin 1 antibody (1:100, Abcam, #ab131551), rabbit polyclonal anti-VAMP2 antibody (1:2000, Abcam, #ab3347), mouse monoclonal anti-SNAP25 antibody (1:5000, Synaptic Systems, #111011), mouse monoclonal anti-Syntaxin 1a antibody (1:2000, Synaptic Systems, #110111), mouse monoclonal anti-Actin antibody (1:5000, Abcam, #ab6276), chicken polyclonal anti-GFP antibody (1:1000, Abcam, #ab13970), rabbit polyclonal anti-GABA antibody (1:1000, Calbiochem, #PC213L), rabbit polyclonal anti-VGLUT1 antibody (1:500, Abcam, #ab104898), monoclonal anti-FLAG M2 antibody (1:200, Sigma, #F1804), purified mouse IgG1 isotype control antibody (BD Pharmingen, #550878). All antibodies were commercially available and validated. References related to the antibodies are listed on the website of the vendors.

10. Eukaryotic cell lines

a. State the source of each eukaryotic cell line used.	We used HEK 293FT (ThermoFisher, R70007) for lentivirus production.
b. Describe the method of cell line authentication used.	We veryfied HEK 293FT by their characteristic shape.
c. Report whether the cell lines were tested for mycoplasma contamination.	Cells were routinely tested for mycoplasma contamination.
d. If any of the cell lines used are listed in the database of commonly misidentified cell lines maintained by ICLAC, provide a scientific rationale for their use.	No commonly misidentified cell lines were used.

Animals and human research participants

Policy information about studies involving animals; when reporting animal research, follow the ARRIVE guidelines

11. Description of research animals

Provide details on animals and/or animal-derived materials used in the study.	We used postnatal day 1 (P1) C57BL/6 pups for primary culture and four-week-old C57BL/6 male mice for lentivirus injection and subject to behavioral studies within two months.

Policy information about studies involving human research participants

12. Description of human research participants

Describe the covariate-relevant population characteristics of the human research participants.	This study did not contain human research participants.